JOURNAL OF MATERIALS SCIENCE 23 (1988) 541–546

Effect of silicon, magnesium, cobalt and iron additions on the microstructure of Al–Li centrifugally atomized powders

FAWZY H. SAMUEL
Central Metallurgical Research and Development Institute, El-Tabbin, Helwan, PO Box Iron and Steel, Cairo, Egypt

G. CHAMPIER
Laboratoire de Physique du Solide, Ecole des Mines, Parc de Saurupt, 54042 Nancy Cedex, France

The effect of the addition of silicon (up to 4 wt%), magnesium (up to 7.25 wt%), cobalt (up to 0.8 wt%) and iron (up to 1.5 wt%) on the microstructure of as-solidified Al–3 wt% Li powders, produced by centrifugal atomization in a helium atmosphere, has been studied by means of optical, scanning electron and transmission electron microscopy. The results show that the microstructure changes from dendritic in the case of Al–Li and Al–Li–Mg alloys to a eutectic (Al + AlLiSi) mixture in the Al–Li–Si alloy to a cellular structure for the Al–Li–Co alloy, and results in the direct nucleation of coarse intermetallic Al_6Fe from the melt followed by subsequent growth in the case of Al–Li–Fe alloy.

1. Introduction

The technique of quenching or rapid cooling of a material from an elevated temperature to room temperature or below, followed by degassing, extrusion and annealing (either at room temperature or elevated temperatures) to develop suitable microstructures and hence desired properties, has received good attention among metallurgists and material scientists. However, quenching treatments have, until recently, been confined to the solid state, the main purpose being either the retention of phases stable only at high temperatures as in precipitation-hardening studies, or the utilization of non-equilibrium transformations as in the production of martensite in steels.

An effective way of improving the strength and ductility of binary Al–Li alloys is to introduce incoherent dispersoid particles and to refine the grain size using the rapid solidification technique. During the annealing of Al–Li binary alloys, soft continuous precipitate-free zones form along the grain boundaries and, hence, early cracks. The importance of the dispersoid particles is to change the mechanism of deformation from inhomogeneous into more homogeneous which, in turn, improves the alloy ductility [1].

In the present work we report on the effect of light elements like silicon and magnesium (with respect to the density of pure aluminium) and heavy metals like cobalt and iron on the microstructure of as-solidified Al–Li powders. Table I shows the expected phases and their densities which ultimately affect the alloy density. The volume fractions of these phases could only be calculated for cobalt and iron elements since they form no compounds with lithium.

2. Experimental procedures

Alloys used in the present study were prepared from high-purity metals (~99.9%) under an inert atmosphere of argon. Rapidly solidified powders were produced by the conventional centrifugal atomizing process, with helium used as the cooling medium. Ingots of 400 g were melted in a graphite crucible having an orifice of 1 mm diameter and coated with a thick layer of boron nitride refractory. The atomizing chamber was evacuated and filled with helium up to 1 bar (10^5 Pa). The liquid metal was ejected on to a rotating atomizer with a helium overpressure. The chemical composition and designation of the alloys are given in Table II.

The microstructures of powder particles (with sizes ranging between 25 and 200 μm) were examined by light microscopy; scanning electron microscopy, (SEM) operating at 14 kV, and transmission electron microscopy (TEM) operating at 200 kV (for details see Samuel [2]). The precipitates were identified by X-ray diffraction using a Co$K\alpha$ source.

All the above-mentioned elements, e.g. lithium, silicon, magnesium, cobalt and iron, form a eutectic

TABLE I Precipitate specifications

System	Precipitation	Structure	Density ($g\,cm^{-3}$)
Al–Li	Al_3Li	Cubic	2.33
Al–Li–Si	AlLiSi	Cubic	1.95
Al–Li–Mg	Al_2MgLi	Cubic	1.85
Al–Li–Co	Al_9Co_2	Monoclinic	3.62
Al–Li–Fe	Al_3Fe	Monoclinic	3.77
	Al_6Fe	Orthorhombic (metastable)	3.45

0022–2461/88 $03.00 + .12

TABLE II Alloy specifications

Designation	Composition (wt % (at %))					Initial pour temperature (°C)
	Li	Si	Mg	Co	Fe	
L3	3 (10.8)	–	–	–	–	800
LS4	2.7 (9.72)	3.78 (4.07)	–	–	–	850
LM5	3.15 (11.34)	–	4.65 (5.5)	–	–	730
LM8	3.25 (11.7)	–	7.25 (8.5)	–	–	800
LC4	3 (10.8)	–	–	0.4 (0.2)	–	800
LC8	3 (10.8)	–	–	0.8 (0.4)	–	800
LF2	2.72 (9.8)	–	–	–	1.3 (0.6)	800

structure with aluminium (binary systems). The eutectic temperature, eutectic composition and maximum solubility at room temperature are given in Table III.

3. Results and discussion

3.1. Al–Li–Si system

Although much information is available about the Al–Li–Fe, Al–Li–Co and Al–Li–Mg systems, a lot less is available concerning the Al–Li–Si system. Therefore, four alloys containing 3% Li* in common with 1, 2, 4 and 8% Si, respectively, were chill-cast. The microstructures were examined by light microscopy. Fig. 1a shows the essential features of Al–3% Li–2% Si, revealing the presence of primary α-Al crystals separated by the eutectic product (Al + AlLiSi phases). Increasing the silicon content up to 4% (Fig. 1b) results in replacing the primary α-Al crystals with primary AlLiSi crystals surrounded by silicon-depleted regions. The rest of the liquid decomposed into the eutectic mixture, constituting about 80% of the microstructure (based on quantitative metallographic measurements). These results, thus, enable us to say that the addition of 3 wt % Li to Al–Si alloys shifts the eutectic point from 12.6 wt % for the binary system to less than 4 wt % for the ternary one.

The microstructure of the powder particle is greatly influenced by the powder particle size. For sizes up to 50 μm, the microstructure (Fig. 2a) reveals a dendritic structure with AlLiSi fine precipitates delineating the secondary dendrite arms. From measurements of the secondary dendrite arm spacing, the cooling rate was determined to be in the range 10^4 to 10^6 K sec^{-1}.

*All percentages in wt %.

Increasing the particle size up to 80 μm (Fig. 2b) produces a microstructure similar to that presented in Fig. 1a for Al–3% Li–2% Si chill-cast alloy. Comparing these two figures highlights the refinement effect of rapid solidification. From the TEM micrograph (Fig. 3) representing a eutectic region, the distance between two AlLiSi lamellae is of the order of 0.1 to 0.2 μm, i.e. one-tenth of the corresponding distance obtained from Fig. 1a. According to the Al–Li equilibrium diagram [3], the maximum solubility of lithium in α-Al is 5 at %. The present alloy contains ~ 10 at % Li (see Table II), whereas the formation of the AlLiSi phase needs 4 at % Li. Therefore, this alloy does not show an effective volume fraction of δ' (Al_3Li) precipitates which are responsible for strengthening the alloy on ageing.

Fig. 2c is the microstructure of powder particle size of the order of 200 μm. The main features in this micrograph are essentially the same as those shown in Fig. 1b for Al–3% Li–4% Si chill-cast alloy. The effect of rapid solidification appears in reducing (i) the amount of primary AlLiSi crystals (~ 7% in Fig. 2b and 20% in Fig. 1b), and (ii) the size of AlLiSi primary crystals from 10 to 50 μm in solid-state alloy to 1 to 3 μm after rapid solidification. Comparing Figs 2b and c emphasizes the extended solid solubility, enhanced by increasing the cooling rate via decreasing the powder particle size.

The above-mentioned results allow us to conclude that if the Si/Li atomic concentration ratio is less than unity, all the silicon is included in the AlLiSi phase. If the lithium concentration is less than 5 at %, lithium remains in solid solution with no occurrence of δ' (Al_3Li) precipitation. Thus, for obtaining an

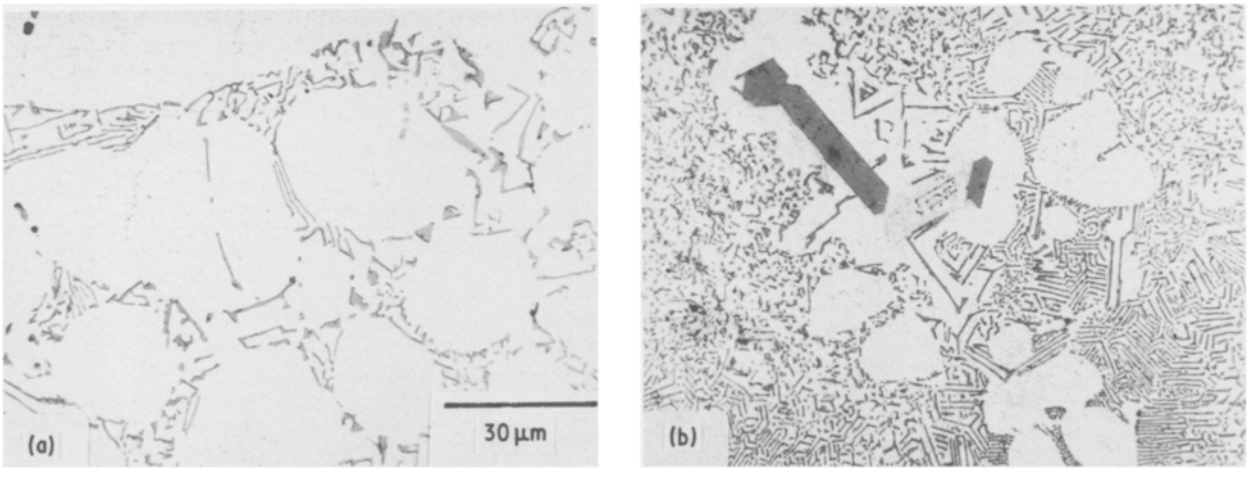

Figure 1 Optical micrographs of chill-cast Al–3 wt % Si alloys: (a) 2 wt % Si, (b) 4 wt % Si. Cooling rate $\dot{T} \sim 10^2$ K sec^{-1}.

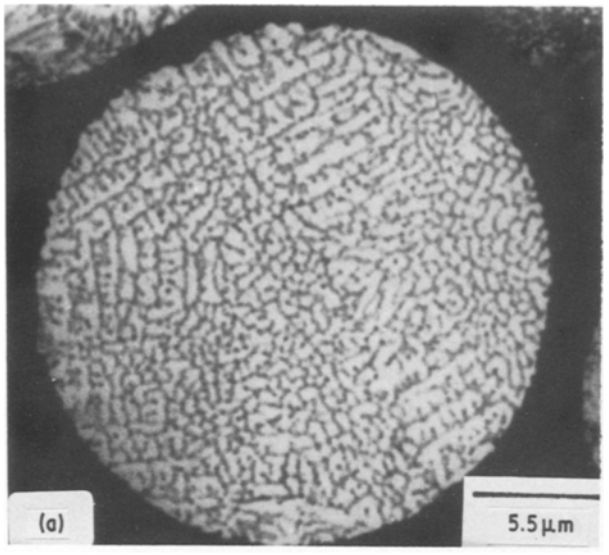

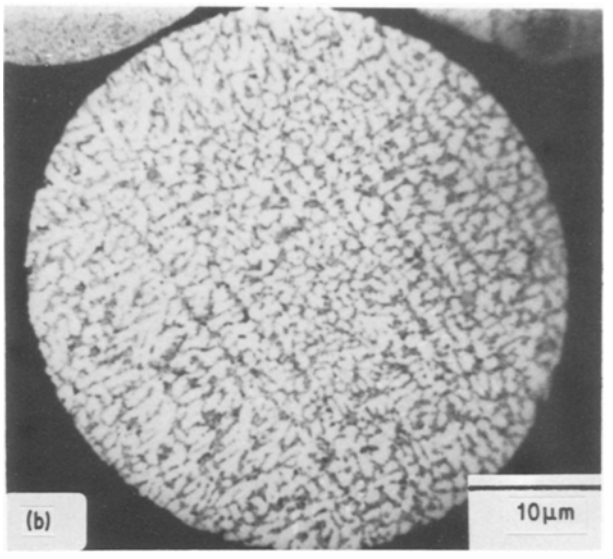

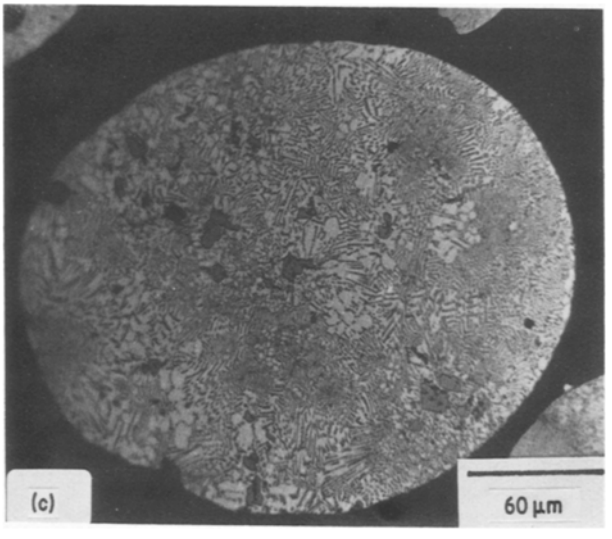

Figure 2 Optical micrographs of LS4 powder of different particle sizes: (a) $\sim 50\,\mu m$, (b) $\sim 80\,\mu m$ ($\dot{T} \sim 10^4$ to $10^6\,K\,sec^{-1}$), (c) $\sim 200\,\mu m$.

appreciable volume fraction of Al_3Li precipitates in the presence of silicon, the concentration of lithium in the alloy should be sufficiently high. This, in turn, reduces further the alloy density (ϱ). According to our density measurements, performed on loose powders containing various concentrations of silicon and lithium, the density of an Al–Li–Si alloy can be expressed by the relation

$$\varrho = 2.7 - 0.24\,C_{Si} - 2.008\,C_{Li}$$

where C_{Si} and C_{Li} are, respectively, the atomic concentrations of silicon and lithium. The expected density of the present alloy is $2.49 \times 10^3\,kg\,m^{-3}$.

3.2. Al–Li–Mg system

Fig. 4 exhibits the two main forms of the powder particles obtained in the present work. One is nearly spherical (A) and the other is partially spherical ending in an elongated part (B).

The volume of a spherical particle (with diameter D_g) equivalent to the volume of an elongated particle is given by the expression

$$V = \frac{\pi D_g^3}{6} = \frac{\pi D_1^2}{4}\,l + \frac{\pi D_2^3}{6}$$

where D_1 is the diameter of the spherical part of B and D_2 is the diameter of the cross-section of the elongated part of B. l is the length of the elongated part.

A direct relation between the secondary dendrite arm spacing (SDAS) and powder particle diameter is obtained for L3, LC8, LM5 and LM8 alloys (Fig. 5). The addition of 4.6% Mg to Al–3% Li (L3 alloy) does not coarsen much the SDAS of L3 alloy as

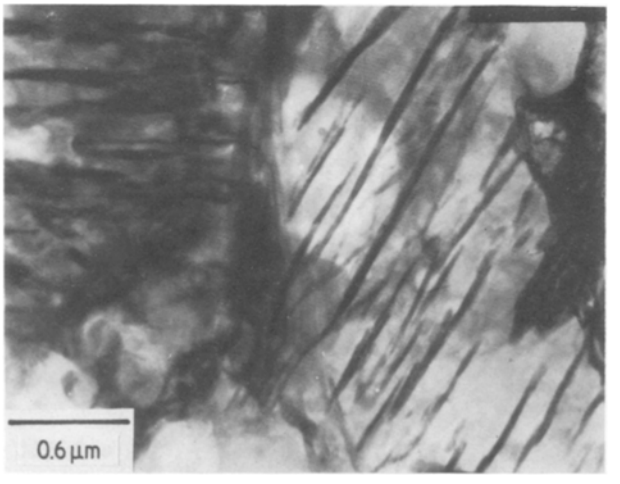

Figure 3 TEM micrograph of a eutectic area corresponding to Fig. 2b.

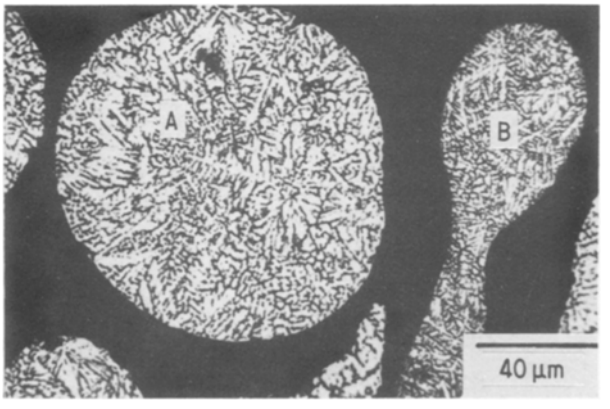

Figure 4 Optical micrograph showing the main forms of powder particle obtained in the present work.

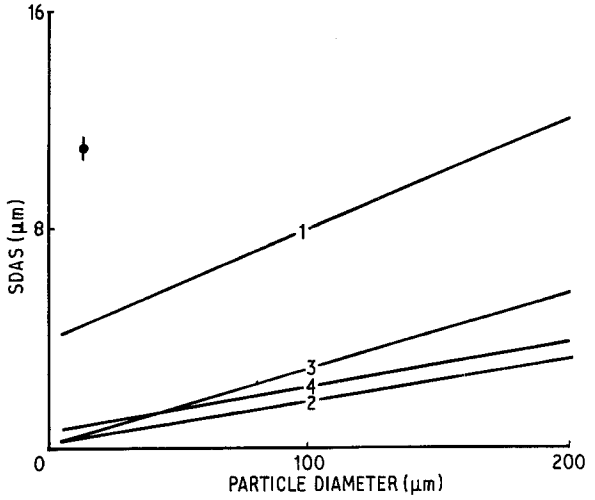

Figure 5 Relationship between secondary dendrite arm spacing (SDAS) and particle diameter. (1) Al–2.7% Li (in argon), (2) L3 and LM8 (helium), (3) LC8 (helium), (4) LM5 (helium). ♦ represents the error margin or scattering.

compared with the remarkable increase in SDAS due to addition of 0.8% Co. Increasing the magnesium content up to 7.5% results in obtaining SDAS values very close to that of L3, i.e. refinement of the SDAS of LM8. These observations explain the influence of heavy precipitates such as Al_9Co_2 and light precipitates like Al_2MgLi on the apparent cooling rates of the powders based on measuring the SDAS.

X-ray diffractometry of both LM5 and LM8 powders indicated the presence of {8 2 2} and {8 4 2} Al_2MgLi reflections in addition to aluminium reflections. Since the size of Al_3Li particles was of the order of 4 μm, they could not be identified by X-ray diffractometry. The work of Harris and co-workers [4, 5] on Al–7.2 at % Li–4.7 at % Mg alloy made by ingot metallurgy and tested at 200° C shows that in all cases the δ' (Al_3Li) structure is stable. At temperatures exceeding 200° C the ternary phase Al_2MgLi precipitates, first at the grain boundaries and then, at high temperatures, within the matrix. This causes the δ' precipitates to redissolve. Thus, the formation of Al_2MgLi in the as-solidified powders is due to the breakdown of α-Al solid solution when the temperature of cooling approaches 250° C.

TABLE III Details of Al–X systems

System	Eutectic composition of X (wt %)	Eutectic temperature (° C)	Maximum solubility (wt %)
Al–Li	9.9	600	1.28
Al–Si	12.6	577	41.00
Al–Mg	35.5	451	40.80
Al–Co	1.0	657	nil
Al–Fe	1.9	655	nil

Fig. 6a is the microstructure of the 150 μm powder particle size of LM5 alloy. As can be seen, solidification occurred by the nucleation of three spherical caps with the interfaces exhibiting axisymmetric

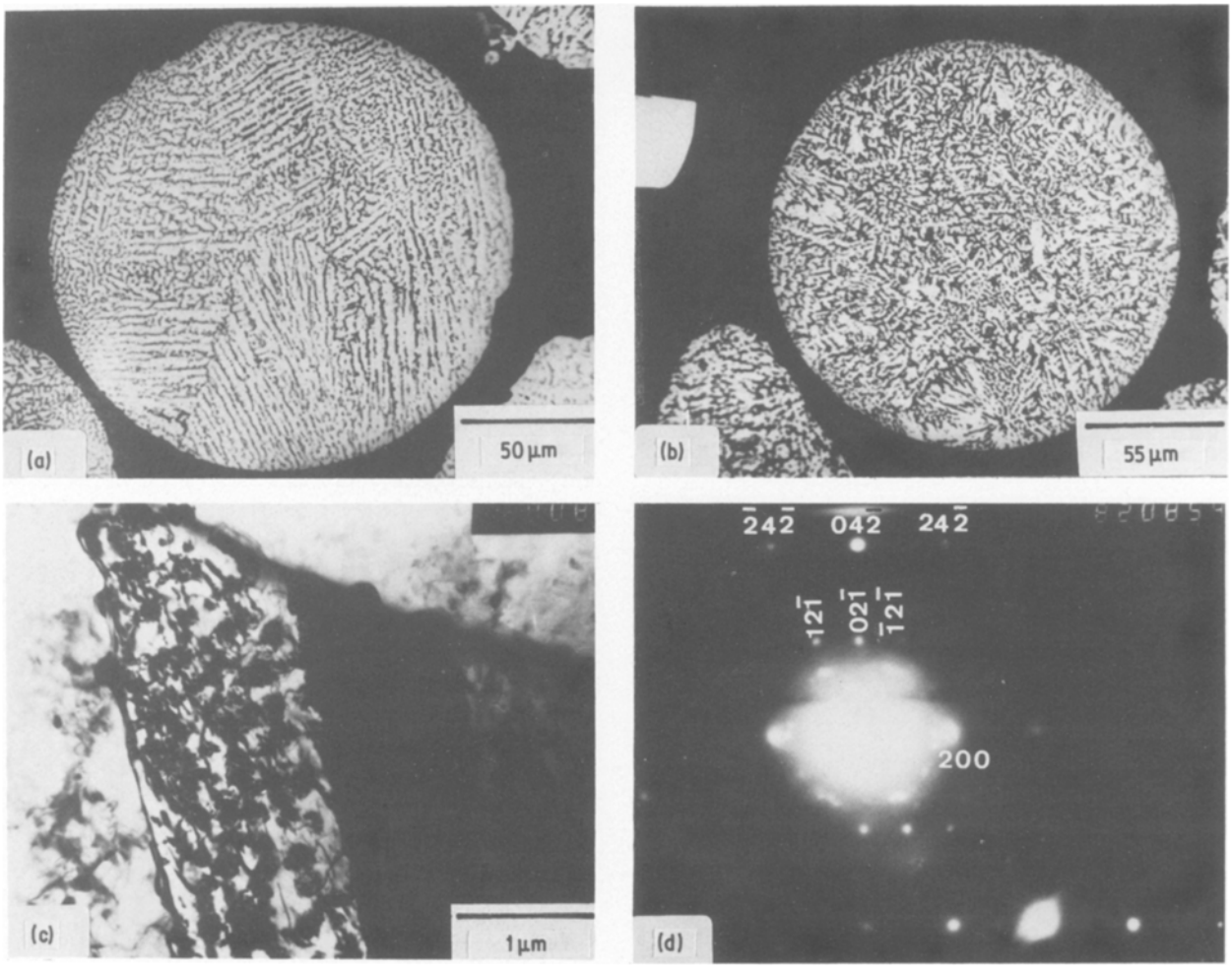

Figure 6 Microstructure of Al–Li–Mg powders: (a) LM5 (optical), (b) LM8 (optical), (c) LM8 (TEM), (d) selected-area diffraction corresponding to (c), indicating the presence of [0 1 2] α-Al and δ' (Al_3Li).

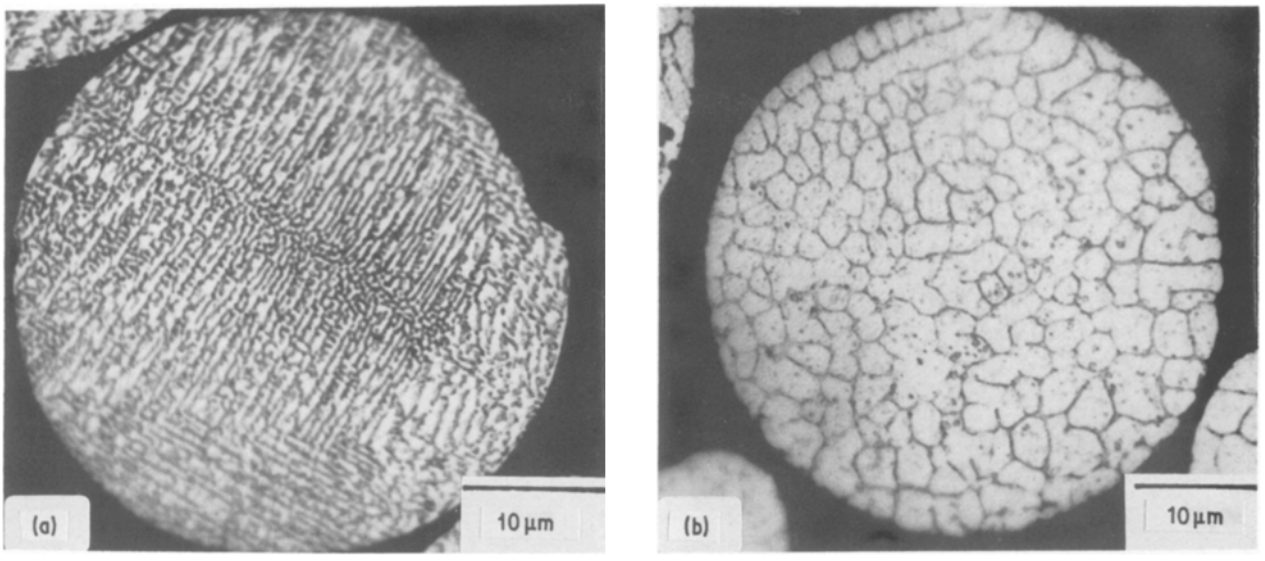

Figure 7 Optical micrographs of 80 μm powder particle size of (a) Al–3 wt % Li, (b) Al–3 wt % Li–0.8 wt % Co.

geometry. These interfaces are not exactly straight due to kinks caused by the dendrite arms on arriving at the boundary. Fig. 6b reveals the microstructure of the 150 μm powder particle size of LM8, bearing similar details as those shown in Fig. 6a. TEM examination of the 100 to 150 μm powder particles of LM8 alloy reveals the presence of Al_2MgLi precipitates decorating the secondary dendrite arms in the as-solidified conditions (Fig. 6c). Under proper tilting conditions, superlattice spots corresponding to δ' (Al_3Li) phase particles could be obtained as shown in Fig. 6d. Thus, not all the lithium content is introduced into the Al_2MgLi phase. In fact, examination of the extruded and solution heat-treated alloy gave strong evidence for the precipitation of Al_3Mg_2 phase particles. In this case, the volume fraction of any phase depends on the lithium partition distribution.

3.3. Al–Li–Co system

The microstructure of Al–3 wt % Li (L3) powder reveals well-defined colonies of dendrites for particles of $\sim 200\,\mu$m as shown in Fig. 7a. These dendrites are comprised of cylindrical arms probably elongating along the three equivalent $\langle 1\,0\,0 \rangle$ directions. In this case the solidification is presumably proceeding as an advancing front that radiates from the initial point of nucleation. Coarse particles $> 200\,\mu$m exhibit a mixed dendritic/equiaxed type of structure. The equiaxed structure was characterized by the absence of directional growth in a polished section.

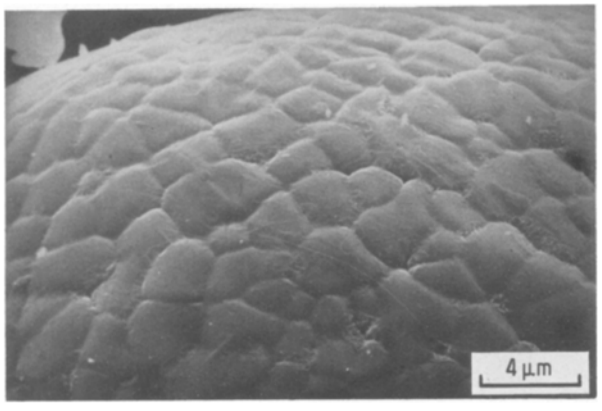

Figure 8 SEM micrograph of LF2 powder.

In the Al–3 wt % Li–0.4 wt % Co powder with a particle diameter larger than 25 μm, a large proportion of the microstructure is cellular. Also, in the Al–3 wt % Li–0.8 wt % Co alloy quenched from 800° C, the cellular structure is predominant, irrespective of particle size (Fig. 7b). We are assuming here that all cobalt will be precipitated in the form of Al_9Co_2 which has a density of $3.6 \times 10^3\,kg\,m^{-3}$. Under these conditions, the volume fraction of Al_9Co_2 precipitates is about 2.25%. What needs to be emphasized is that the partitioning of intermetallic Al_9Co_2 particles may reduce the stability of a planar liquid–solid interface, leading to cellular undulations during cooling of a superheated liquid alloy droplet. For this the G_L/R ratio (G_L = thermal gradient in liquid, R = interface velocity) should be high enough to allow the transition from dendritic to cellular structure for a given cooling rate.

As the droplet recalesces, the interface velocity (R) and undercooling are reduced. When the interface temperature goes above the temperature required for supersaturation, solute is rejected ahead of the interface. This process breaks the stability of the interface and favours cell formation. The solute in the intercellular regions has a higher supersaturation. This gives rise to nucleation of Al_9Co_2 in the liquid ahead of the interface. Now, for the trapping of an Al_9Co_2 particle by a moving interface, the nucleated particles must possess a certain critical size for a given interfacial velocity [2]. Based on the present TEM investigations, these are, respectively, 30 to 40 nm and $5 \times 10^4\,m\,sec^{-1}$. Below the critical size, the particles will be pushed by the moving interface. For example, the size of particles in the Al_3Li phase is about 4 nm and they are segregated into the secondary dendrite arms.

3.4. Al–Li–Fe system

Fig. 8 is a typical microstructure of LF2 powders. The absence of a growth direction makes us believe that the microstructure is mainly comprising cells or

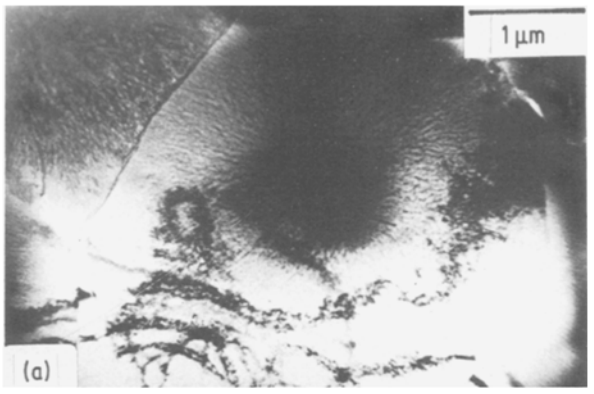

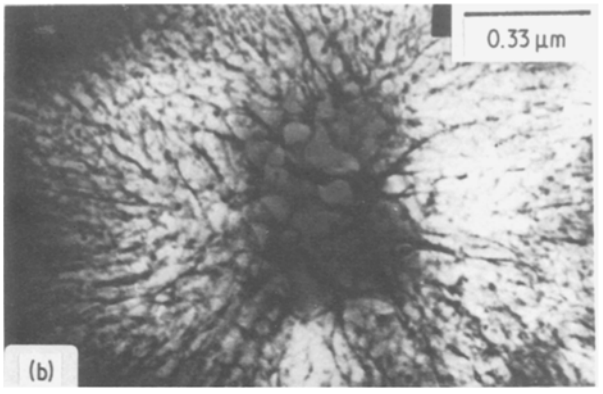

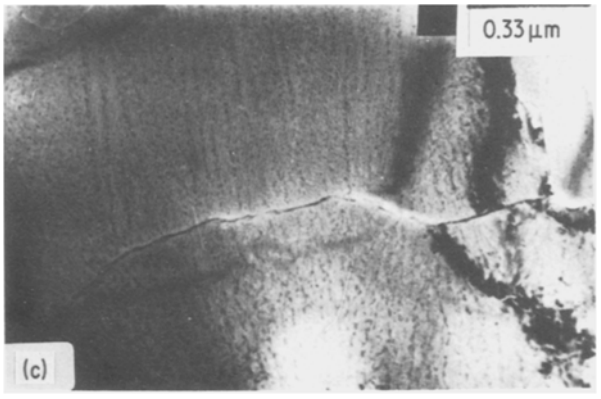

Figure 9 (a–c) TEM micrographs of different magnifications, corresponding to Fig. 8.

grains. The sides of these grains are not always straight. The TEM micrographs in Figs 9a to c are obtained from the powder particles shown in Fig. 8. Near to the centre of each grain, a coarse particle of Al_6Fe (as could be identified from analysing the corresponding electron diffraction pattern) can be seen. The nucleation and growth of primary Al_6Fe is followed by the subsequent nucleation and growth of primary aluminium dendrite arms. This primary aluminium is found to grow radially outward from the central intermetallic. The secondary dendrite arms are delineated by the precipitation of both Al_3Li and Al_3Fe particles.

Jones [6] has reported a similar observation in a rapidly solidified Al–11 wt % Fe hypereutectic alloy made by melt spinning. He refers to this microstructure as Zone B, and it is characterized by coarse intermetallics surrounding primary aluminium dendrites. It should be noted that the intermetallics appear to be located at the centres of local solidification fronts. This would suggest that the intermetallic was the first solid to nucleate and grow, followed by primary aluminium and not the reverse.

When a hypoeutectic aluminium alloy initially solidifies, primary aluminium is expected to nucleate first, especially at high rates of solidification that can suppress the nucleation of the intermetallics. Therefore, we believe that in coarser powder particles, the primary intermetallic Al_6Fe nucleates at pre-existing clusters in the liquid at temperatures above the liquidus rather than at random sites during the undercooling of the liquid prior to solidification [7]. As the temperature drops, the growth of the intermetallic halts due to reduction in the rate of solute transport, and primary aluminium then fills in the area surrounding the intermetallics. The front containing both Al_6Fe and α-Al grows radially outward until it runs into another solidification front.

4. Conclusions

The present observations made on the microstructure of centrifugally atomized Al–3 wt % Li–X powders, where X = Si, Mg, Co and Fe, can be summarized as follows:

1. Binary Al–Li alloy exhibits a dendritic microstructure and over the entire range of selected particle size, 25 to 200 μm.
2. Addition of 3 wt % Li to the Al–Si system shifts the eutectic point to less than 4% Si. The eutectic structure is a mixture of aluminium and AlLiSi phases. Increasing the cooling rate, through reducing the powder particle size, increases the extent of solid solubility.
3. Addition of magnesium up to 7.25 wt % does not change either the dendritic morphology or the secondary dendrite arm spacing. The main advantage of magnesium addition is the reduction in alloy density due to the precipitation of Al_2MgLi.
4. Addition of cobalt in quantities up to 0.8 wt % changes the dendritic structure of Al–3 wt % Li into complete cellular structure, regardless of the powder particle size.
5. Addition of iron in quantities up to 1.5 wt % leads to the formation of coarse Al_6Fe intermetallic from the melt, followed by subsequent growth.

References

1. T. H. SANDERS Jr, E. A. LUDWICZAK and R. R. SAWTELL, *Mater. Sci. Eng.* **43** (1980) 247.
2. F. H. SAMUEL, *Met. Trans.* **17A** (1986) 73.
3. D. B. WILLIAMS, in Proceedings of 1st Conference on Aluminium–Lithium Alloys, Stone Mountain, May 1980 (TMS-AIME, 1981) p. 89.
4. B. NOBLE, S. J. HARRIS and K. HARLOW, in Proceedings of 2nd Conference on Aluminium–Lithium Alloys, Monterey, April 1983 (TMS-AIME, 1984) p. 65.
5. S. J. HARRIS, B. NOBLE and K. DINSDALE, *ibid.* p. 219.
6. H. JONES, *Mater. Sci. Eng.* **5** (1969/70) 1.
7. R. K. GARRETT and T. H. SANDERS Jr, *ibid.* **60** (1983) 269.

Received 2 March
and accepted 29 April 1987